Range-Sensitive Bayesian Passive Sonar Tracking

Bryan A. Yocom, **Jason M. Aughenbaugh**, and **Brian R. La Cour**
Applied Research Laboratories
The University of Texas at Austin
P.O. Box 8029, Austin, Texas 78713-8029 USA
{byocom, jason, blacour}@arlut.utexas.edu

Abstract – *Passive sonar arrays are commonly operated under a far-field assumption in which the only observable parameter regarding target location is the direction of arrival of the target's signal. Range can be observed, but only when a target is in the near-field region of the array. In a Bayesian formulation of the problem, additional range dependence may be added to the passive sonar likelihood function by utilizing knowledge of the source level of a target of interest. It is shown that incorporating such knowledge of source level can increase track accuracy, both in the near-field and far-field regions of the array. In addition, it is shown that source level modeling can give a field of omni-directional sensors the ability to detect and localize a target.*

Keywords: Bayesian tracking, grid-based, passive sonar, range dependence

1 Introduction

The majority of passive sonar arrays are operated under a far-field assumption. That is, the sources are assumed to be far enough from the array that their received wavefronts can be well approximated by a plane wave. As a result, the only observable parameter regarding target location is the direction of arrival (DOA), or bearing, of the signal. If the target is to be localized, one must either use multiple arrays [1, 2] or, if the array is moving, use its motion to localize the target [2, 3].

When targets are in the near-field region of the array one can exploit the wavefront curvature to additionally estimate the range to the target [4, 5]. In order for the array to have a reasonably sized near-field region, the aperture of the array must be very large or the frequency of the target's signal very low. Even though an array may have a significantly sized near-field region, its detection region may be even larger. One would hope that if a target were to move from the near-field region to the far-field region that a previously built up range estimate would be maintained. A tracker may have a tendency to choose the range that is farthest from the array because the area of each bearing sector increases with range from the array. Oftentimes this range estimate is not reasonable because it corresponds to a target source level (SL) that is much larger than one would expect for a given type of target of interest (TOI).

Therefore, we propose adding additional range dependence to the passive sonar likelihood function by making modest assumptions on the SLs one expects to hear from a TOI. The additional range dependence can be included when doing near-field or far-field beamforming. In addition, this range dependence can be used to give omni-directional sensors the ability to detect and localize a target when the background noise power is assumed known. This is similar to the approach taken in [6]. Here, we treat the propagation model as deterministically known and the SL as probabilistically known. In [6], the TOI's SL is assumed to be deterministically known whereas the propagation model is known probabilistically. Both approaches have the effect of introducing additional uncertainty in the range estimate.

A grid-based Bayesian tracker is used to both detect and track a single TOI in a variation of a track-before-detect system. Such an approach has been shown to properly characterize the highly non-Gaussian measurement errors and ambiguities inherent to passive sonar [1, 2]. Fundamentally, it assumes that the uncertainty in our knowledge of the state of the target (or targets) may be represented well by probabilities. Bayes' theorem then provides the basic mechanism whereby measurements update these probabilities and, hence, our state of knowledge of the world. The probabilities serve as a common interface for different sensors, and thus the problem of data fusion becomes one of modeling the probabilities for different sensors. An alternative to the grid-based approach would be to represent the TOI's probability density function (PDF) using Gaussian mixtures [7, 8].

In this paper we, we demonstrate that *a priori* assumptions on the source level of a TOI can be used to increase the range dependence of the passive sonar likelihood function, both when performing near-field and far-field beamforming. We begin in Section 2 with a background on Bayesian tracking, passive sonar data modeling, and the common bearing only likelihood function. In Section 3 we introduce range dependence to our likelihood function via near-field beamforming and modeling of the target source level. Next, Section 4

considers various simulated examples involving a long linear array and distributed fields of omni-directional sensors. We conclude in Section 5 with a brief summary.

2 Background

2.1 Grid-based Bayesian Tracking

Described now is a principled Bayesian approach to the problem of detecting and tracking a single target of interest (TOI). In our approach we consider a state space which consists of the the number of targets present (either zero or one in this paper) and the target's kinematic state, $\mathbf{s}$, given that a target is present. The quantity p_m will represent the probability that a single target is present in a particular region of interest after the mth measurement is incorporated, where $m = 0$ corresponds to the prior distribution. The PDF, defined on this region of interest, will be represented by $\rho_m(\mathbf{s})$.

In order to represent the continuous PDF on kinematic state, $\mathbf{s}$, in a computer, it must be either parametrized, as in Kalman filters [9], or discretized, as in particle filters [10] and grid-based methods [11, 2, 1, 12]. In this paper, we adopt a grid-based implementation, based on the details in an article that is under review [13]. The goal in this approach is to calculate the probability that the target is in each of the grid cells. Fundamentally, this is a piece-wise constant approximation of the PDF. Measurement updates using a grid-based approach are very easy, as they only require a point-wise multiplication of the prior PDF with the likelihood function. The likelihood value for each cell is computed by integrating over the dimensions of that cell to obtain an average likelihood. Currently this integral is approximated by taking the average of a set of uniformly distributed samples in a cell. This effectively performs the non-linear mapping from measurement space (typically range/bearing) to the TOI state space, $\mathbf{s}$ (typically Cartesian).

Two likelihood functions are relevant. The target likelihood function $L_m(\mathbf{x}_m|\mathbf{s})$ denotes the likelihood of receiving measurement $\mathbf{x}_m$ given that the target is in state $\mathbf{s}$. The no-target likelihood function $L_m(\mathbf{x}_m|\varnothing)$ denotes the likelihood of receiving measurement $\mathbf{x}_m$ when there is no target present. Measurement updates on the kinematic PDF are performed using Bayes' theorem, which for notational purposes we write as

$$\rho_m(\mathbf{s}) = L_m(\mathbf{x}_m|\mathbf{s})\,\rho_m^-(\mathbf{s})\,/E_m, \tag{1}$$

where ρ_m^- is the motion updated prior distribution and E_m is the partial Bayesian evidence [14] for a target being present, where E_m is given as

$$E_m \equiv \int L_m(\mathbf{x}_m|\mathbf{s})\,\rho_m^-(\mathbf{s})\,\mathrm{d}\mathbf{s}. \tag{2}$$

Similarly, the target probability is updated by

$$p_m = \frac{E_m p_m^-}{\left(1-p_m^-\right)L_m(\mathbf{x}_m|\varnothing) + p_m^- E_m}, \tag{3}$$

where p_m^- is the motion updated target probability. Derivations of these recursive relations may be found in [11].

The motion model used in this paper is based on the assumption that the targets follow a dynamically based birth/death process [15] where the underlying dynamics are based on an Integrated Ornstein- Uhlenbeck (IOU) process [11]. The motion update is implemented using a particle-filter-like model in which each grid cell is sampled with particles, and then the IOU model is used as in [10] to update the particle cloud for each cell. Then, the particles and their associated probability weights are aggregated back into the grid representation. Additional details are provided in [13].

2.2 Measurement Data Modeling

It is assumed that there is at most one target radiating an acoustic pressure signal onto an N-element array (although the model presented below can be generalized to account for multiple targets as in [2]). The target and sensors are all assumed to be at the same depth. The target is assumed to behave as a point source that emits spherical waves. When the shortest distance from a sensor to the target is greater than $2L^2/\lambda$, where L is the array aperture and λ is the wavelength of the received signal, then the target is said to be in the far-field of the array. When a target is in the far-field its received signal can be well approximated by a planar wave-front [16]. The only observable parameter regarding target location is therefore the direction of arrival (DOA) of the plane-wave signal, which we will denote as ϕ.

The far-field assumption is very common in the field of array processing. In fact, the well-known reference on array processing, [16], contains only a few short paragraphs discussing near-field sources. When a target is in the near-field of the array, the wavefront curvature can be exploited to perform range estimation. The radius of the near-field region of the array increases with the square of the array aperture and inversely with the wavelength. Since it is not uncommon for passive sonar arrays to be hundreds of meters long, it would seem reasonable to exploit wavefront curvature. For example, a 221 meter long array operating at 200 Hz has a near-field region that goes out roughly 13 km. Of course, the $2L^2/\lambda$ distance is not a hard cutoff but rather a rule of thumb. Although the range of a target will not suddenly become observable at this distance, one can expect a significantly large area in which the range of a target is potentially observable.

The frequency domain model which we will use for the sampled array output is given by $N \times 1$ vector,

$$\mathbf{x}(k_f, k_t) = s(k_f, k_t)\,\mathbf{v}(k_f, \phi, r) + \mathbf{n}(k_f, k_t), \tag{4}$$

where k_f represents the frequency snapshot index, k_t is the time snapshot index, $s(k_f, k_t)$ is the signal amplitude at the phase center of the array, $\mathbf{v}(k_f, \phi, r)$ represents the the so-called array manifold vector to a signal in direction ϕ at range r, and $\mathbf{n}(k_f, k_t)$ is additive noise. The array manifold vector represents the phase shift (and possibly amplitude scaling) of the signal at each sensor relative to the signal received at a reference "phase center", which for notational simplicity we have assumed to be at the origin. The range and bearing of the target in (4) are also referenced to this phase

center. Processing will be performed on K_f frequency snapshots about the signal's center frequency, resulting in a total of $K \equiv K_f K_t$ data snapshots. A measurement will be represented by the variable $\mathbf{x} = \left\{ \mathbf{x}(k) \,\middle|\, k = 1, 2, ..., K \right\}$, where k represents a generic index over data snapshots. Frequency dependence will be dropped from notation from this point forward because it is assumed that the signal's center frequency is known.

2.3 Statistical Model

It is assumed that the signal and noise are mutually independent, zero-mean Gaussian random processes with variance σ_{s}^2 and σ_{n}^2, respectively. Based on the model of (4), and assuming that the signals are uncorrelated, the observation data covariance matrix has the form

$$\mathbf{R}_{\mathbf{x}}(\mathbf{s}) = E\left\{ \mathbf{x}(k)\, \mathbf{x}(k)^H \right\} \tag{5}$$

$$= \sigma_{\text{s}}^2 \mathbf{v}(\phi, r)\, \mathbf{v}(\phi, r)^H + \sigma_{\text{n}}^2 \mathbf{I} \tag{6}$$

where σ_{s}^2 and σ_{n}^2 represent the received signal and noise powers, respectively. Note that there is a non-linear relationship between the target state, $\mathbf{s}$, and the range and bearing. A quantity commonly required in many signal estimation procedures is the sample covariance matrix,

$$\mathbf{C}_{\mathbf{x}} = \frac{1}{K} \sum_{k=1}^{K} \mathbf{x}(k)\, \mathbf{x}(k)^H \tag{7}$$

where $(\cdot)^H$ represents the conjugate transpose matrix operator. Based on our assumptions, the log-likelihood function (LLF) is given by [16]

$$\ln L(\mathbf{x}|\mathbf{s}) = -NK \ln(\pi) - K \ln\left(|\mathbf{R}_{\mathbf{x}}(\mathbf{s})|\right) - K \text{tr}\left(\mathbf{R}_{\mathbf{x}}^{-1}(\mathbf{s})\, \mathbf{C}_{\mathbf{x}}\right). \tag{8}$$

By substituting the form for $\mathbf{R}_{\mathbf{x}}(\mathbf{s})$, given by (6), into (8) and removing the constant $-NK \ln(\pi)$ we obtain the simplified expression

$$\ln L(\mathbf{x}|\mathbf{s}) = B(\mathbf{x}) - K \ln\left(1 + \beta(\phi, r) \frac{\sigma_{\text{s}}^2}{\sigma_{\text{n}}^2}\right) + K \left(\frac{1}{\sigma_{\text{n}}^2} \cdot \frac{\beta(\phi, r)^2 \frac{\sigma_{\text{s}}^2}{\sigma_{\text{n}}^2}}{1 + \beta(\phi, r) \frac{\sigma_{\text{s}}^2}{\sigma_{\text{n}}^2}} \right) P_{\text{CBF}}(\phi, r) \tag{9}$$

where

$$P_{\text{CBF}}(\phi, r) = \frac{\mathbf{v}(\phi, r)^H \mathbf{C}_{\mathbf{x}} \mathbf{v}(\phi, r)}{\beta(\phi, r)^2}, \tag{10}$$

$$\beta(\phi, r) = \mathbf{v}(\phi, r)^H \mathbf{v}(\phi, r), \tag{11}$$

and

$$B(\mathbf{x}) = -K \left[\frac{1}{\sigma_{\text{n}}^2} \text{tr}(\mathbf{C}_{\mathbf{x}}) + N \ln\left(\sigma_{\text{n}}^2\right) \right]. \tag{12}$$

The function $P_{\text{CBF}}(\phi, r)$ is the output power of a conventional beamformer (CBF) [16]. Unfortunately, the parameters σ_{s}^2 and σ_{n}^2 are usually not known *a priori*. To that end, the parameters are replaced with their maximum likelihood estimates (MLEs) when evaluating (9) as done in [2, 17]. These MLEs can be found using an alternating maximization algorithm such as that outlined in [2]. When no target is present ($\sigma_{\text{s}}^2 = 0$) the no-target log-likelihood is given by

$$\ln L(\mathbf{x}|\varnothing) = B(\mathbf{x}). \tag{13}$$

Note that in practice the constant $B(\mathbf{x})$ does not need to be calculated because it can be subtracted out of $\ln L(\mathbf{x}|\mathbf{s})$ and $\ln L(\mathbf{x}|\varnothing)$. This normalization has no effect on the measurement update performed in (1) and (3).

2.4 Bearing-Only Likelihood Function

If a target is assumed to be in the far-field of the array, the LLF, (9), is evaluated as a function of bearing only. In this case the nth element of the manifold vector is given by [16]

$$v_n(\phi) = \exp\left[j \frac{2\pi}{\lambda} \epsilon(x_n, y_n, \phi) \right] \tag{14}$$

where

$$\epsilon(x_n, y_n, \phi) \equiv x_n \cos(\phi) + y_n \sin(\phi), \tag{15}$$

x_n and y_n are the x and y location of the nth array element, respectively, and λ is the signal wavelength. The LLF then simplifies to the form commonly seen:

$$\ln L(\mathbf{x}|\mathbf{s}) = B(\mathbf{x}) - K \ln\left(1 + N \frac{\sigma_{\text{s}}^2}{\sigma_{\text{n}}^2}\right) + K \left(\frac{N}{\sigma_{\text{n}}^2} \cdot \frac{N \frac{\sigma_{\text{s}}^2}{\sigma_{\text{n}}^2}}{1 + N \frac{\sigma_{\text{s}}^2}{\sigma_{\text{n}}^2}} \right) P_{\text{CBF}}(\phi) \tag{16}$$

where

$$P_{\text{CBF}}(\phi) = \frac{\mathbf{v}(\phi)^H \mathbf{C}_{\mathbf{x}} \mathbf{v}(\phi)}{N^2}. \tag{17}$$

In the next section, we develop two methods for incorporating range dependence into the likelihood models.

3 Likelihood Function with Range Dependence

In this section we will investigate two ways of adding range dependence to the bearing-only LLF of (16). One method, range focused beamforming, simply exploits the natural structure of the signals received at the array elements, as outlined in Section 2.2. It does not require *a priori* knowledge of any signal parameters, but it is only effective at observing the range of a target when the target is in the near-field of the array. Another, more novel method, is to exploit *a priori* knowledge regarding the target's source level (SL) to localize it in range. Since the SL of a target is not usually known exactly we will characterize our knowledge of SL in terms of a PDF.

3.1 Near-field Beamforming

In the most general case, $v_n(\phi, r)$ is given by [4, 5]

$$v_n(\phi, r) = \frac{r}{r_n} \exp\left[-j\frac{2\pi}{\lambda}(r_n - r)\right] \quad (18)$$

where

$$r_n = \sqrt{r^2 + d_n^2 - 2r\epsilon(x_n, y_n, \phi)} \quad (19)$$

is the distance from the nth array element to the source and

$$d_n^2 \equiv x_n^2 + y_n^2. \quad (20)$$

This array manifold vector accounts for both the phase difference and amplitude scaling between the various sensors. Note that it is slightly different than the one given in [4, 5] because we have defined $s(k_f, k_t)$ in (4) to be the signal at the phase center of the array, not the signal at the source.

Ideally, we would like $v_n(\phi, r)$ to maintain a stable form even as $r \to \infty$ (i.e. the source is in the far-field of the array). It is not clear from (18) that this is the case. After substituting in (19), (18) can be rearranged to obtain the final form for the array manifold vector:

$$v_n(\phi, r) = \frac{1}{\gamma(r, \phi, x_n, y_n)} \times \exp\left[-j\frac{2\pi}{\lambda}\left(\frac{\frac{d_n^2}{r} - 2\epsilon(x_n, y_n, \phi)}{\gamma(r, \phi, x_n, y_n) + 1}\right)\right]. \quad (21)$$

where

$$\gamma(r, \phi, x_n, y_n) = \sqrt{1 + \frac{d_n^2}{r^2} - \frac{2\epsilon(x_n, y_n, \phi)}{r}} \quad (22)$$

Note that in the limit as $r \to \infty$, (21) simplifies to (14). This array manifold vector therefore has a stable form even as $r \to \infty$.

3.2 Range Dependence via Source Level Modeling

Assuming that the target behaves as a point source and that there is no attenuation, refraction, or reflections, the source signal will experience spherical spreading. The received signal power, σ_s^2, is then related to the SL, S, by $\sigma_s^2 = S/r^2$. We can substitute this relation into (16) in order to re-parametrize the LLF to be in terms of range and SL:

$$\ln L(\mathbf{x}|\mathbf{s}) = B(\mathbf{x}) - K\ln\left(1 + N\frac{S}{r^2\sigma_n^2}\right) + K\left(\frac{N}{\sigma_n^2}\cdot\frac{N\frac{S}{r^2\sigma_n^2}}{1 + N\frac{S}{r^2\sigma_n^2}}\right)P_{\text{CBF}}(\phi). \quad (23)$$

When using this LLF we will assume we have some knowledge of the SL. The noise power is still a nuisance parameter and is therefore replaced with its MLE as before. The maximum of this equation, for a fixed bearing and SL assumption, can be found to be

$$r_{\max} = \sqrt{\frac{S}{P_{\text{CBF}}(\phi) - \frac{\sigma_n^2}{N}}}. \quad (24)$$

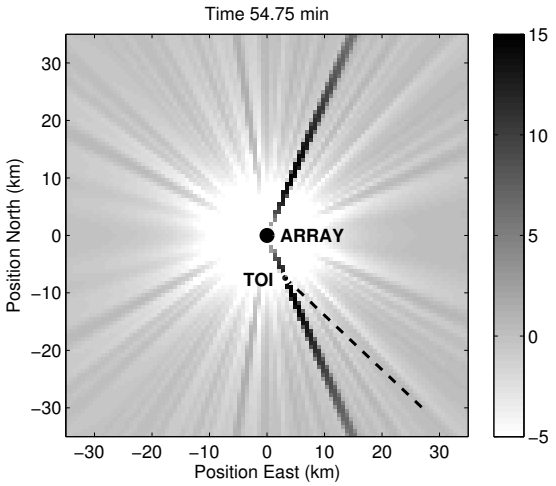

Figure 1: An example log-likelihood function for an east-west oriented linear array with known SL from the scenario in Section 4.1. The locations of the array and target are indicated by a solid circle and open circle, respectively. The no-target log-likelihood is zero.

An example of this sort of LLF is shown in Fig. 1 and Fig. 2 for the scenario discussed later in Section 4.1. In this figure the modeled SL matched the true SL. At the bearing of the TOI, $67.0°$, the LLF is peaked near the TOI and falls off both at close and far range. At other bearings, where $P_{\text{CBF}}(\phi) > \frac{\sigma_n^2}{N}$, there are small peaks above the no-target log-likelihood. At bearings where $P_{\text{CBF}}(\phi) < \frac{\sigma_n^2}{N}$, there are no peaks above the no-target log-likelihood, as indicated by (24). It is seen in Fig. 1 that the log-likelihood values at bearings besides the TOI are very low for close range. This is because the estimated received signal power at these bearings is consistent with the target being at a far range. Note that the uncertainty in range is a direct result of the true form of the LLF. Although it is commonly assumed that the uncertainty in range can be well represented by a Gaussian or sum of Gaussians [7, 8, 6, 18], we see here that it is often a poor approximation.

Our assumptions on source level therefore have a clear impact on our range estimate. Unfortunately, one does not usually have knowledge of the exact SL of a target of interest (TOI). A more reasonable assumption would be to say that the target could have a range of source levels. This knowledge can be characterized in the form of a PDF on S, $\rho(S)$. For this paper we have assumed a uniform distribution on SL, in units of dB re: $1\mu\text{Pa}^2$/ Hz, between S_{low} and S_{hi}. The parameter S in (23) can then be marginalized out (assuming SL is independent of range and bearing):

$$L(\mathbf{x}|\mathbf{s}) = \int \rho(S)\, L(\mathbf{x}|\phi, r, S)\, \mathrm{d}S. \quad (25)$$

This integral is approximated with a summation over a set of

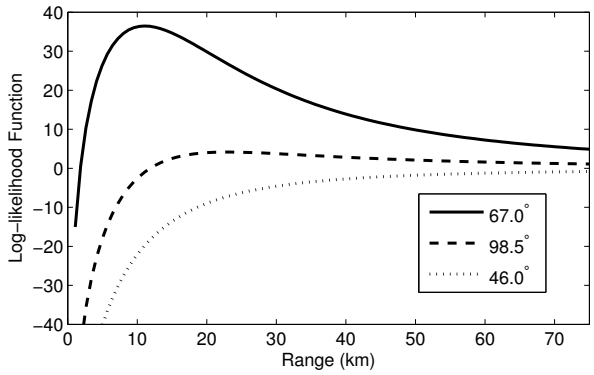

Figure 2: An example log-likelihood function in range for particular bearings for an array with known SL from the scenario in Section 4.1. The TOI is at 67.0° and a range of 8.05 km. The no-target log-likelihood is zero.

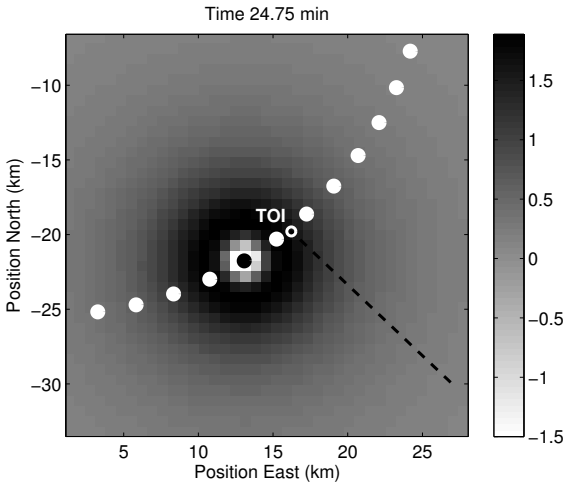

Figure 3: An example log-likelihood function for an omni-directional sensor with known SL and noise power from the scenario in Section 4.2.1. Solid circles indicate sensor locations, with the black solid circle representing the sensor which this measurement corresponds to. The target location is indicated by an open circle. The no-target log-likelihood is zero.

L SLs that are linearly spaced in dB:

$$L\left(\mathbf{x}|\mathbf{s}\right) = \frac{1}{L}\sum_{l=1}^{L} L\left(\mathbf{x}|\phi, r, S_l\right) \tag{26}$$

where $S_1 = S_{\text{low}}$ and $S_L = S_{\text{hi}}$. With this approximation we are effectively averaging over a range of SLs.

For demonstrative purposes, we also consider a sensor which has only one element. The LLF, (23), simplifies to

$$\ln L\left(\mathbf{x}|\mathbf{s}\right) = B\left(\mathbf{x}\right) - K\ln\left(1+\frac{S}{r^2\sigma_{\text{n}}^2}\right) + K\left(\frac{1}{\sigma_{\text{n}}^2}\cdot\frac{\frac{S}{r^2\sigma_{\text{n}}^2}}{1+\frac{S}{r^2\sigma_{\text{n}}^2}}\right)\mathbf{C}_{\mathbf{x}}. \tag{27}$$

where the maximum of this equation occurs at

$$r_{\max} = \sqrt{\frac{S}{\mathbf{C}_{\mathbf{x}} - \sigma_{\text{n}}^2}}. \tag{28}$$

Clearly, this sensor is now omni-directional. That is, it has no ability to observe the bearing of the target. Another complication is that the noise power can no longer be replaced by its MLE because the ability to estimate the noise power relies on the directionality of an array [2]. Therefore, in order to use this LLF one must have *a priori* knowledge of the noise power. An example of this sort of LLF is shown in Fig. 3 for the scenario discussed later in Section 4.2.1. In this figure the modeled SL and noise power matched the true SL and noise power. The LLF has an annular shape which is peaked near the range of the TOI.

Since *a priori* knowledge of the noise power is required for omni-directional sensors, we should investigate the sensitivity to this parameter. Shown in Fig. 4 is a LLF for various noise power assumptions. It should be clear that the the LLF is quite sensitive to assumptions on noise power. Underestimating the noise power does not harm our ability to localize the target very much (when the target is detectable), but, as will be shown later, it will cause problems with false alarms. In this example overestimating the noise power by 3 dB causes the entire LLF to fall below the no-target log-likelihood. As seen in (3), this will cause the target probability to drop regardless of the shape of the prior PDF.

It is also instructive to visualize the effects of averaging over a range of source levels. Fig. 5 shows LLFs for various SL assumptions and a LLF averaged over these SLs. There are a couple interesting effects that result from averaging over source level. First, the peak of the average LLF is much broader than the peaks of any of the individual LLFs. This is a desirable effect because we want to maintain high likelihood over an interval of ranges so that we do not "miss" the target. Second, the height of the average LLF is lower than the height of any of the individual LLFs. Since we have introduced uncertainty in SL, the likelihood at each range should, indeed, be reduced. A third, more subtle effect, is found where the peak in the average LLF occurs. Although the average LLF appears to be quite flat over the range of interest, it is in fact, not. There is no guarantee that this peak will occur at the location of the target. If a target is stationary the resulting peak in the PDF will become sharper and sharper after each measurement until the target appears to be highly localized, possibly in the incorrect location. This effect is not as strong when the target is moving because the peak will tend to move in range as the target moves. Although the effects of SL averaging were discussed for an omni-directional sensor, the same effects are present when the sensor is an array.

One can, of course, combine range focusing and SL modeling. This simply amounts to replacing N and $P_{\text{CBF}}\left(\phi\right)$ in (23) with $\beta\left(\phi, r\right)$ and $P_{\text{CBF}}\left(\phi, r\right)$, respectively. The maxi-

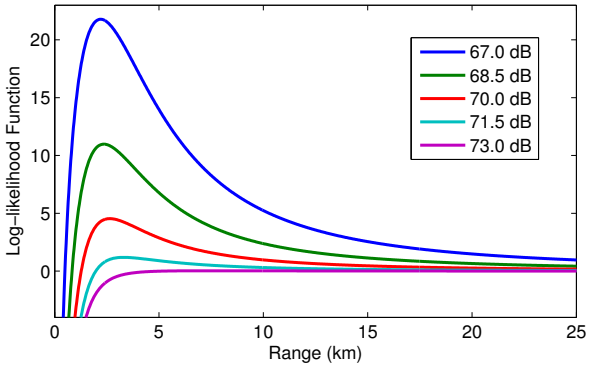

Figure 4: Log-likelihood function for an omni-directional sensor for various noise power assumptions. The true noise power is 70.0 dB. The true SL is 139.3 dB and is assumed known. The true range of the target is 3.7 km. The no-target log-likelihood is zero.

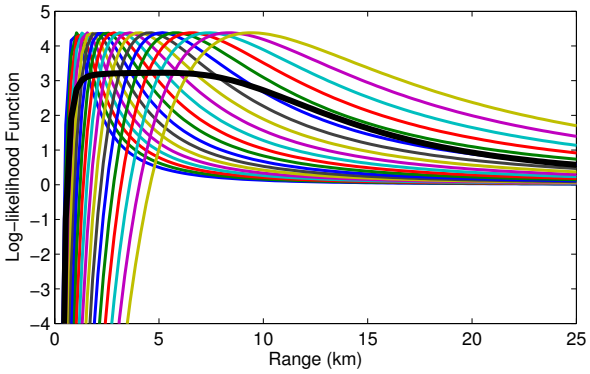

Figure 5: Log-likelihood function for an omni-directional sensor for various SL assumptions. The LLFs for SLs between 130 and 150 dB are shown in color. The LLF averaged over these SLs is black. The true SL is 139.3 dB. The true noise power is 70.0 dB and is assumed known. The true range of the target is 3.7 km. The no-target log-likelihood is zero.

mum of this likelihood function does not necessarily occur at the range defined by (24) because of the additional range dependence in β and the CBF output power.

4 Examples

A set of examples are now considered which demonstrate the flexibility of grid-based Bayesian tracking with passive sensors. Each example will have 61 sensor elements but configured in very different manners. There is interest in surveilling a circular region with a radius of 22.5 km. In each of the various sensor configurations we wish to investigate the trade-offs between early detection, track accuracy, and required *a priori* knowledge. The target will be the same in all examples. Fig. 6 outlines the various sensors configurations and shows the target trajectory. The black line located at the origin represents a 221 m long linear array that is oriented

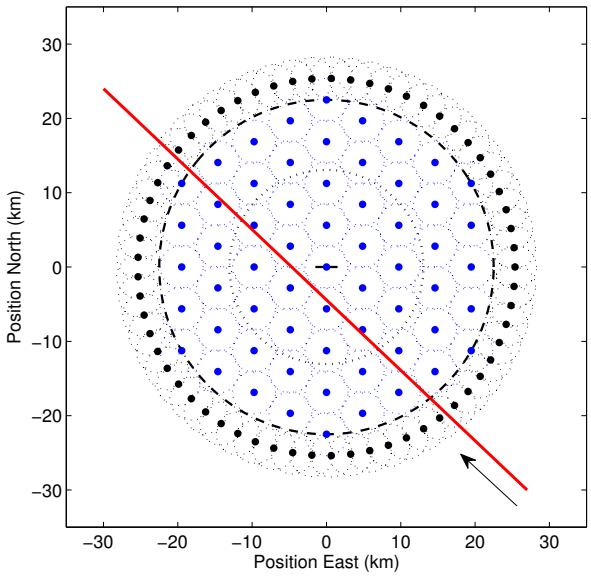

Figure 6: Three different sensor configurations for tracking a target with the trajectory given by the red line.

east-west. The large dashed and dotted black circles represent the near-field region and detection region, respectively, for the array. The detection region of the array also corresponds to the circular region of interest. The blue dots represent a field of omni-directional sensors distributed on a hexagonal grid with detection regions given by dotted blue circles. The black dots and circles also represent omni-directional sensors which are instead distributed along a circle that is outside of the region of interest. The radii of the detection regions are derived from the true source level and noise power (i.e. a target can only be detected if the received SNR is greater than one).

Element-level time series data was generated using the Sonar Simulation Toolset (SST) [19]. The acoustic environment assumes there are no reflections, and the sound speed profile is constant with $c = 1500$ m/s. The target emits a narrowband acoustic signal and moves in a straight line from (27, -30) km to (-30, 24) km with a speed of 10 m/s. Its power spectrum is normally distributed with a mean of 200 Hz and a standard deviation of 3 Hz. It is assumed that the frequency of interest, 200 Hz, is known *a priori*. Measurements are processed in 30-second scans with a sampling rate of 2400 Hz and 16384-point FFT windows. Three frequency bins were shared when computing the sample covariance matrix. The average source level and noise power across the frequency bins processed were 139.3 and 70.0 dB, respectively.

The state space is bounded from -35 to 35 km east and north in position and from -12 to 12 m/s east and north in velocity. Position is represented on a 101×101 grid. Since passive sonar provides minimal velocity information, the velocity state space is represented over only 1 grid cell. This approximation essentially assumes a uniform distribution in velocity at all times. It is not necessary to make this assumption,

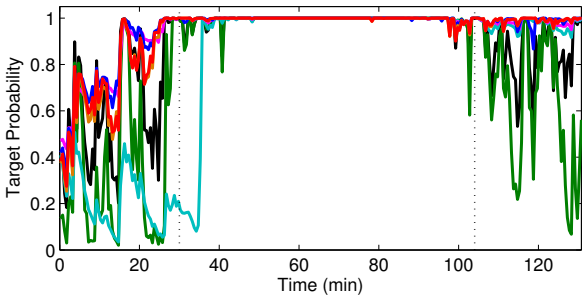

Figure 7: Probability of target presence when using the array. Color legend is included in Fig. 8. Times when the target enters and leaves the sensor detection regions are denoted with dotted black lines.

but having a one-dimensional state space in velocity does significantly improve computation time. We have found acceptable performance when making this assumption and processing only passive sonar measurements.

4.1 One Long Array

The first example considers a 61 element, 221 m long uniformly-spaced horizontal line array (HLA) that is oriented east-west at the origin. The array has a far-field distance of $2L^2/\lambda = 13$ km. The DOA of each signal is measured relative to the line of bearing of the array (i.e., 0° is forward endfire and 90° is broadside). Note that when a linear array is used the DOAs from 0° to 180° are indistinguishable from those at 180° to 360°. This is often referred to as left-right ambiguity. The array is therefore not able to totally localize the target. The PDF will properly represent the left-right ambiguity of the array by maintaining probability mass on each side of the array.

Results for the array are shown in Fig. 7 and Fig. 8. Plots of the RMS error in position are not shown because the left-right ambiguity of the array makes it impossible to determine which side of the array the target is on. Instead, Fig. 8 shows the estimated range and bearing of the target as a function of time, where estimates are formed by choosing the maximum *a posteriori* (MAP) estimate of the PDF.

The most basic likelihood function is one which uses far-field beamforming and does not model the SL. For this case we are able to do a very good job of estimating the bearing and declaring a high probability of target presence when the target is within the detection region of the array. As one would expect, the range estimate is very poor. Due to the geometry of the problem, the range is initially estimated as being very large. This is an effect of discretizing our PDF into a grid. Since bearing sectors cover a larger area in Cartesian space as range increases, they are more likely to fully cover a grid cell at far range than close range. As the target moves closer to the array we are able to do a better job of estimating its range. This can be attributed to the motion model. The TOI velocity is assumed to fall within -12 to 12 m/s east and north. Because the TOI has a large bearing rate when it is close to the array, the only way a target can exist at a far range is for it to have a velocity which is greater than that modeled. The probability of being at a far range is, therefore, correctly lowered. When the target leaves the detection region the target probability drops some and we begin to incorrectly estimate bearing.

When near-field beamforming is performed we are able to obtain comparable performance in target detection and bearing estimation, but are able to do a better job in range estimation when the target is in the near-field region. Notice that the range is not accurately estimated until the target is in the near-field region for some time. This is because it takes some time for the probability mass to move from far range to close range. When the target leaves the near-field region the range estimate quickly become erroneous. This would indicate that the geometric preference to choose the farthest range, discussed earlier, overpowers the fact that probability mass has collected around the true range of the TOI.

Modeling the SL to be uniformly distributed between a range of values has a number of interesting effects on detection and estimation performance. We first consider the use of far-field beamforming. When the SL is modeled as 110-150 dB there is little change in range estimation performance. Detection and bearing estimation, however, change significantly. The target is not detected with a probability near one until about 36 min, which is about 9 min later than without SL modeling. This is also noticeable as a delay in accurate bearing estimation. The reason for this effect is because we have averaged over a large range of SLs. As discussed in Section 3.2, averaging over a range of SLs will cause the maximum of the LLFs to be smaller than when either a single SL is used or SL is not modeled at all. It therefore takes a longer time for the tracker to decide with certainty that there is a target. Similarly, it will take a longer time for the tracker to determine that there is not a target once the target probability is high. This is why we are able to maintain an accurate bearing estimate through the end of the scenario and why the target probability remains so high. A more subtle point is that when not modeling the SL a large portion of the probability mass is near the boundary of the state space. Since the motion model assumes that this probability mass may leave the region of interest, corresponding to a target "death," the probability of target presence drops accordingly.

As the range of modeled SLs is tightened, we are able to do a better job of estimating the range of the target while maintaining good detection and bearing estimation performance. The estimated range is no longer always chosen as the farthest point from the array, because this point would correspond to a SL which is higher than the range of SLs averaged over. The tightest ranges of SLs chosen is 135-140 dB, which should roughly correspond to the SLs we expect to hear. This range of SLs leans toward the lower end of the true SL (139.3 dB) because the radiated spectrum of the target will contain some unmodeled Doppler shift due to target movement. Since the frequency band used is fixed and centered about 200 Hz we should expect the estimated SL to be lower than the true SL.

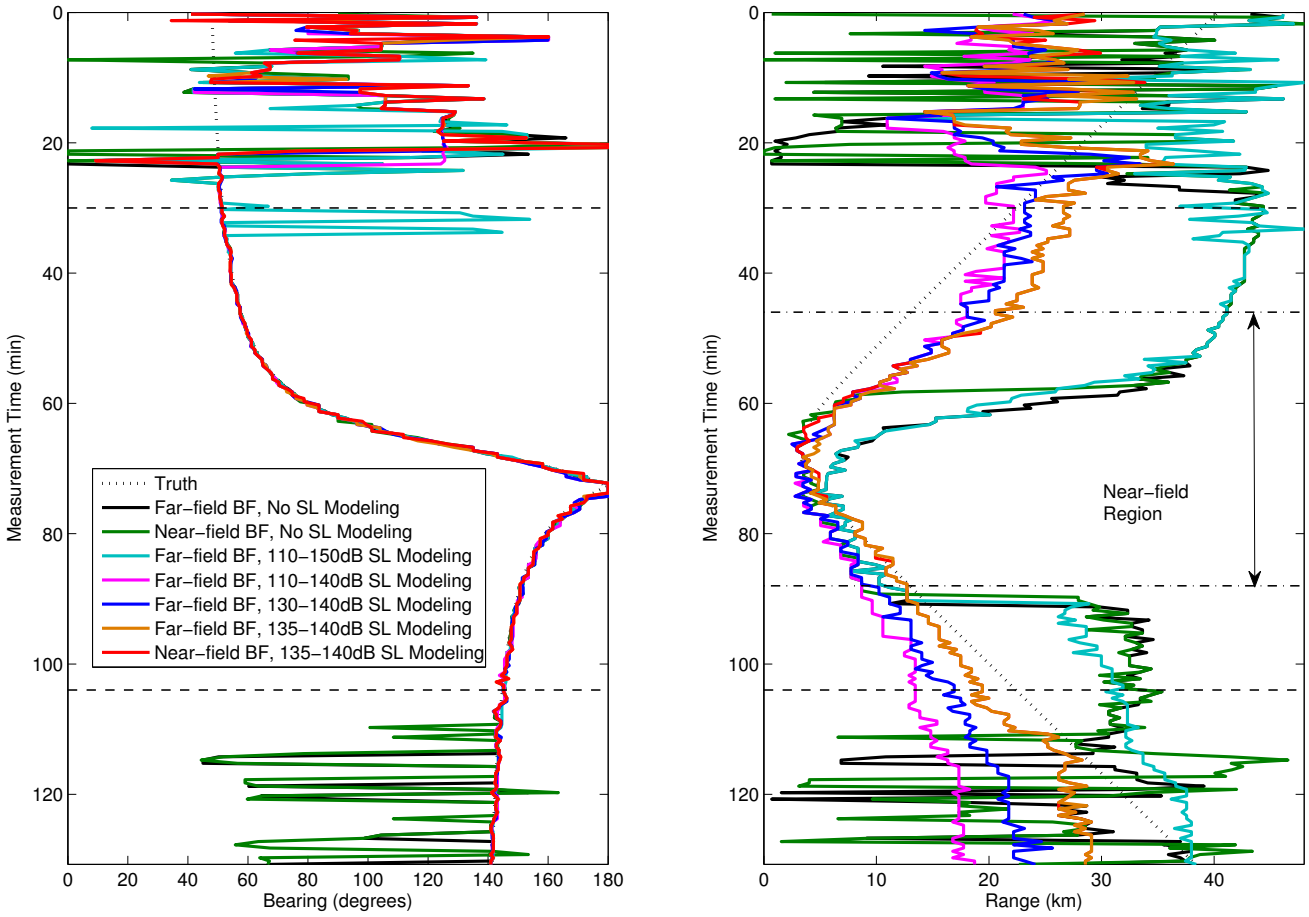

Figure 8: Estimated bearing and range when using the array. Results are shown for various types of beamforming (BF) and SL PDFs. Times when the target enters and leaves the sensor detection regions are denoted with dotted black lines.

Finally, we consider averaging over SLs from 135-140 dB while also performing near-field beamforming. As one might expect, we are able to obtain slightly better range estimation in the near-field region of the array, particularly at the closest ranges. Since near-field beamforming is effectively inactive when the target is at far range, the range estimation performance is nearly identical to when far-field beamforming was performed.

4.2 Distributed Omni-Directional Sensors

The next two examples will each use 61 omni-directional sensors (i.e. single element sensors). In both of these examples the SL of the target is assumed to be well known and in the range 135-140 dB. Performance is investigated for various noise power assumptions, as this is a required input parameter. The true noise power is 70.0 dB.

4.2.1 Sensors Behaving as a Tripwire

In this example the sensors are distributed uniformly along a circle of radius 25.4 km. The goal of this distribution is to provide an early detection on whether a target exists. If the region within the circle has already been determined to not contain a TOI, these sensors could be used as a sort of tripwire to warn when a target is entering the region of interest. If a detection is declared, then another type of sensor system, such as active sonar, could be cued to operate.

Results are shown in Fig. 9. When the modeled noise power matches the true noise power, the tracker behaves as one would expect. Before the target enters the first detection region, it cannot be localized. The target probability is relatively low but fluctuates because of randomness in the noise. When the target enters the first detection region, the target probability quickly rises to one and the target is well localized. As the target leaves the detection regions, the RMS error rises and the target probability drops slightly, but never near zero. This is actually the behavior one should expect.

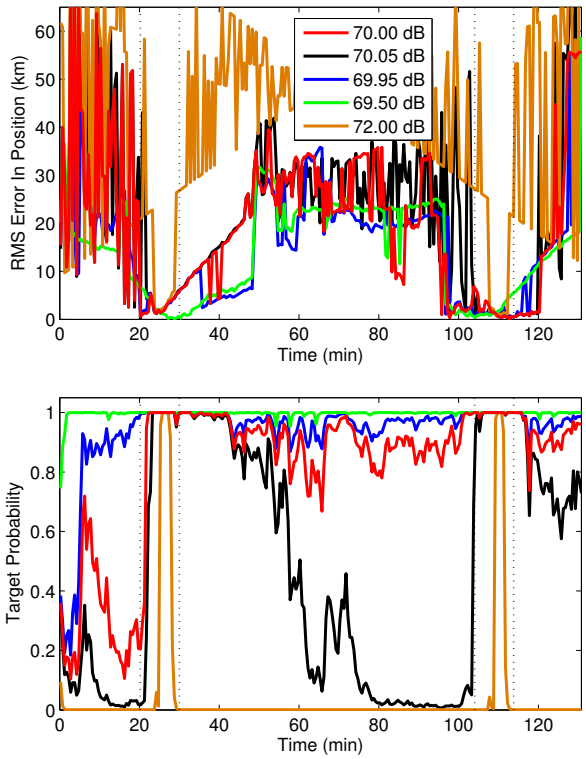

Figure 9: RMS error in position and probability of target presence for omni-directional sensors behaving as a tripwire. Results are shown for various noise power assumptions. SLs are modeled as 135-140 dB. Times when the target enters and leaves the sensor detection regions are denoted with dotted black lines.

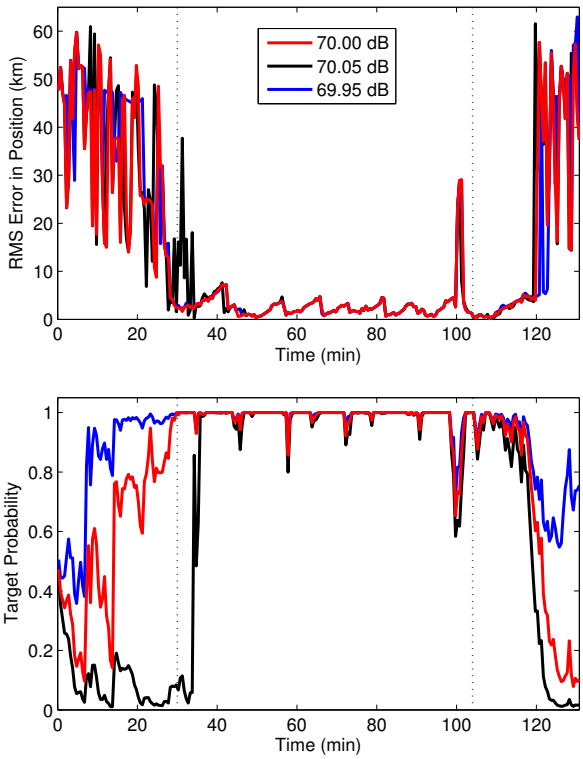

Figure 10: RMS error in position and probability of target presence for uniformly distributed omni-directional sensors. Results are shown for various noise power assumptions. SLs are modeled as 135-140 dB. Times when the target enters and leaves the sensor detection regions are denoted with dotted black lines.

Since each sensor is no longer able to detect the target, they should all have LLF values that approach the no-target log-likelihood at far range. Since the majority of the probability mass will be near these farther ranges, the partial Bayesian evidence, (2), will have a value near the no-target log-likelihood. Analysis of the measurement update of the target probability, (3), shows that for this value the target probability should not change much. When the target enters the second detection region, we have similar behavior.

Underestimating and overestimating the noise power causes two separate types of problems. If the noise power is overestimated, the target probability drops to zero even though there are certain regions of the TOI state space that the sensors cannot "see". Fortunately, the sensors are spaced closely enough that the target is still detected and localized when it crosses each detection region. If the noise power is modeled as much higher than 72 dB, the target may not be detected at all. When the noise power is underestimated, the target is falsely declared as detected before it is in the detection regions. The tracker is still able to properly localize the target when it enters the detection region and maintains a good estimate longer than the other scenarios. Although not shown here, the PDF is also highly localized around the target when it is in the region of interest, but relatively spread out when it is not. Of most concern here is the high sensitivity to knowledge of the noise power. Since the same noise power assumption is made across 61 sensors, a difference of only 0.05 dB can have a large cumulative effect.

In comparison to Section 4.1, these distributed sensors do indeed provide earlier detection. The trade-off is required knowledge of the noise power and an inability to track the target when it is in the region of interest. Of course these sensors could be distributed on a circle of larger radius to provide even early detection, but the larger spacing would increase the probability of a missed detection.

4.2.2 Uniformly Distributed Sensors

Finally, an example is considered in which the sensors are distributed uniformly in the region of interest. The sensors are equally spaced on a hexagonal grid as this provides optimal coverage of the region. The goal of this distribution is to show that omni-directional sensors can be used to track a target.

Results are shown in Fig. 10. We see here, again, the high sensitivity to knowledge of the noise power. A difference of 0.05 dB causes a substantial change in the estimated target probability. When the modeled noise power matches the true noise power, the target is well localized and detected just as it enters the detection region. It is then able to track the target

fairly well in the detection region, with fairly regular rises in RMS error when the target is in a position that is far from two or more sensors. The large rise in RMS error at 100 min, for example, occurs when the target is in a position of minimal sensor coverage, as can be seen in Fig. 6. Underestimation and overestimation of the noise power causes early and late detection, respectively.

5 Summary

Grid-based Bayesian tracking provides a natural framework for target tracking and detection when sensors have non-Gaussian measurement errors. Passive sonar arrays are able to observe bearing and, when a target is in the near-field of the array, range. We extended the passive sonar likelihood function to be able to estimate the range of a target even when it is in the far-field of the array. This was accomplished by incorporating *a priori* knowledge regarding the target's source level. Source level modeling was also used to give omni-directional sensors the ability to estimate target range when the background noise power is known.

Three examples were considered. The first example used a line array. It was demonstrated that source level modeling can be used to increase the ability of the array to estimate range outside of the near-field region and to increase range estimation accuracy when the target is inside the near-field region. In the second example a field of omni-directional sensors, equal to the number of array elements from the first example, were distributed along the periphery of the region of interest. They were able to provide an earlier detection than the array and give some localization information that might be used as a cue for another type of sensor. The final example had a field of uniformly distributed omni-directional sensors. These sensors were able to detect and track a target through a region of interest with an initial detection time that was comparable to the array.

Acknowledgments

This work was supported by the Office of Naval Research under contract no. N00014-06-G-0218-01.

References

[1] C. M. Kreucher, B. Shapo, and R. Bethel, "Multitarget detection and tracking using multi-sensor passive acoustic data," in *Proc. IEEE Aerospace Conference*, Mar. 2009, pp. 1–16.

[2] B. A. Yocom, B. R. La Cour, and T. W. Yudichak, "A Bayesian approach to passive sonar tracking in the presence of interferers," *IEEE J. Ocean. Eng.*, 2010, under review.

[3] B. La Scala and M. Morelande, "An analysis of the single sensor bearings-only tracking problem," in *Proc. 11th Int. Conf. on Information Fusion*, Cologne, Germany, 2008, pp. 1–6.

[4] Y.-D. Huang and M. Barkat, "Near-field multiple source localization by passive sensor array," *IEEE Trans. Antennas Propag.*, vol. 39, no. 7, pp. 968–975, Jul. 1991.

[5] H.-S. Hung, S.-H. Chang, and C.-H. Wu, "3-D music with polynomial rooting for near-field source localization," in *Proc. IEEE International Conference on Acoustics, Speech, and Signal Processing ICASSP-96*, vol. 6, May 1996, pp. 3065–3068.

[6] R. L. Streit and M. J. Walsh, "Bearings-only target motion analysis with acoustic propagation models of uncertain fidelity," *IEEE Trans. Aerosp. Electron. Syst.*, vol. 38, no. 4, pp. 1122–1137, Oct. 2002.

[7] T. R. Kronhamn, "Bearings-only target motion analysis based on a multihypothesis Kalman filter and adaptive ownship motion control," *IEE Proc. - Radar, Sonar and Navigation*, vol. 145, no. 4, pp. 247–252, Aug. 1998.

[8] D. Mušicki, "Bearings only single-sensor target tracking using Gaussian mixtures," *Automatica*, vol. 45, no. 9, pp. 2088–2092, Jun. 2009.

[9] Y. Bar-Shalom and T. E. Fortmann, *Tracking and Data Association*. Boston, MA: Academic Press, 1988.

[10] M. Arulampalam, S. Maskell, N. Gordon, and T. Clapp, "A tutorial on particle filters for online nonlinear/non-Gaussian Bayesian tracking," *IEEE Trans. Signal Process.*, vol. 50, no. 2, pp. 174–188, Feb. 2002.

[11] L. D. Stone, T. L. Corwin, and C. A. Barlowe, *Bayesian Multiple Target Tracking*. Boston, MA: Artech House, 1999.

[12] J. M. Aughenbaugh, B. A. Yocom, and B. R. La Cour, "Active clutter reduction through fusion with passive data," in *Proc. 13th Int. Conf. on Information Fusion*, Edinburgh, UK, Jul. 2010, under review.

[13] J. M. Aughenbaugh and B. R. La Cour, "Measurement-guided likelihood sampling for grid-based Bayesian tracking," *ISIF Journal of Advances in Information Fusion (JAIF)*, 2009, under review.

[14] D. J. C. MacKay, "Bayesian interpolation," in *Neural Computation*, vol. 4, no. 3, May 1992, pp. 415–447.

[15] B. R. La Cour, "Stationary priors for Bayesian target tracking," in *Proc. Int. Conf. on Information Fusion*, Cologne, Germany, Jul. 2008.

[16] H. L. Van Trees, *Detection, Estimation, and Modulation Theory, Part IV, Optimum Array Processing*. New York: Wiley, 2002.

[17] B. A. Yocom, T. W. Yudichak, and B. R. La Cour, "Bayesian passive sonar tracking in the presence of known interferers," in *Proc. 12th Int. Conf. on Information Fusion*, Seattle, WA, Jul. 2009.

[18] T. Luginbuhl and C. Hempel, "Converting bearings-only measurements to cartesian coordinates," *IEEE Trans. Aerosp. Electron. Syst.*, vol. 45, no. 1, pp. 393–404, Jan. 2009.

[19] R. P. Goddard, "The sonar simulation toolset, release 4.1: Science, mathematics, and algorithms," Applied Physics Laboratory, University of Washington, Seattle, Tech. Rep. APL-UW 0404, Oct. 2002.